Edge Detection Techniques in 3D Electrical Resistivity Data; A Case Study for Depth to Bedrock Investigation at Doi Suthep Foothill Area, Chiang Mai, Thailand

Pimabsorn Ruxnark *[a,b] and Suwimon Udphuay [b]
[a] Boonbadan Partnership Limited, Phitsanulok 65000, Thailand.
[b] Department of Geological Sciences, Chiang Mai University, Chiang Mai 50200, Thailand.
*Author for correspondence; e-mail address: pimabsorn.rn@gmail.com

ABSTRACT

Electrical resistivity tomography (ERT) survey was applied to investigate the depth to bedrock in the Office of Regional Livestock 5, Chiang Mai, located at the foot of Doi Suthep Mountain in Mueang Chiang Mai district, Chiang Mai province. 2D ERT data were collected on a total of 11 parallel lines. Each line is 200 m long and the line separation is 10 m. All the 2D ERT data were collected using 5-m electrode spacing and a gradient electrode configuration. The 2D ERT data of all 11 lines were combined and the combined 3D ERT data were inverted to create 3D ERT inversion models. Two of edge detection techniques; the steepest gradient and the Laplacian were applied in the inverted 3D ERT data to obtain more accurate depth estimation of the bedrock. The steepest gradient method finds the steepest value of the first derivatives of the model while the Laplacian method searches for values of zero in the second derivatives of the model. The Laplacian zero-line correlated with the abrupt changes (i.e., the edge) in the inverted 3D ERT data. Comparison between results from both edge detection techniques, geological data, and groundwater wells has revealed that the depths of the bedrock from the first derivative method in x, y, and z directions and only in z (vertical) direction to the 3D ERT data are more accurate than the depth of bedrock from the second derivative method.

Keywords: bedrock detection, edge detection, electrical resistivity tomography (ERT), 3D ERT

1. INTRODUCTION

The depth of the bedrock is an important factor in determining the strength of a structure's foundation, and thus for structural designing process, especially in earthquake-prone areas. There are several methods of estimating the depth of the bedrock, including wash borings, core drillings and geophysical methods. Wash borings and core drillings give more accurate results than geophysical methods. However, the first two methods with limit. They can give information at a single point only [1]. If the construction area is large, it is necessary to have data from multiple boreholes in order to get comprehensive information on the area for accurate design. This makes it very costly and time consuming. Geophysical surveys, although provide less accurate data than the first two methods, can provide the bedrock depth under a large area in less time and at a lower cost.

Electrical resistivity tomography (ERT) is an electrical geophysical surveying method that relies on the electrical resistivity (ER) properties of Earth materials. The ER of these materials is influenced by the types of minerals, solid bedrock, sediments, air, and water-filled structures, resulting in detectable ER contrasts compared to the surrounding medium [2]. For this study, ERT is chosen as the preferred method for determining the depth to bedrock due to the expected significant ER contrast between the unconsolidated sediments and the underlying bedrock.

The ERT survey uses an electric current (I) released into the subsurface through one pair of electrodes and the resultant voltage potential (V) measured across another pair of electrodes. This measurement can determine the ER of the subsurface. Numerous electrodes can be arranged along a transect, and the modern ERT survey equipment is used to automatically switch the transmitting and receiving electrode pairs through a single multi-core cable connection [3]. The modern ERT survey equipment can measure the electrical properties of the ground in 2D and 3D and has been effectively image subsurface structures and stratigraphy without excavation [4].

To better distinguish between bedrock and sediments in the resistivity model, edge detection techniques were applied. Edge detection is an image processing technique used to identify points in a

digital image that are discrete. The area with the most significant variation is seen as an edge by the edge detection technique. In applying the edge detection technique to the resistivity model data, the area where have the sharply change in resistivity is the boundary between the bedrock and the sediment [5,6]. There are several techniques for edge detection such as Canny edge detector, Kovalevsky. Two popular methods were chosen in this study: (1) steepest gradient method and (2) Laplacian method. The steepest gradient method uses a variation in gradient (first derivative) of the inverted 3D ERT data in the vertical (z) and horizontal (x, y) directions. The Laplacian method finds the zero in the Laplacian (second derivative) of the inverted 3D ERT data in 1) the horizontal (x and y) and the vertical directions (z), and 2) only the vertical direction (z). The Laplacian zero line can accurately determine the edge between sediment and bedrock.

The aim of this study is to apply the two edge detection methods to estimate the depth of the bedrock in 3D ERT data. The results were compared between the two edge-detection techniques with geologic data and groundwater well data to validate the depth of the bedrock, in the hope that this study can be useful to the construction industry or can be used in conjunction with other studies in the future.

2. STUDY AREA

The study area is in the Office of Regional Livestock 5, Chiang Mai (ORLCM), which is located in Mueang Chiang Mai district of Chiang Mai province. The ORLCM area is a part of the Wiang Chet Lin ancient city. Wiang Chet Lin city was built in the year 1411. Wiang Chet Lin is located at the foot of Doi Suthep Mountain in the northwest of Chiang Mai city. The seven waterways flow from Doi Suthep through the city and flank both the north and the south of the city are the origin of the city's name, which means City of 7 Rivers. The specialty of the Wiang Chet Lin is that a canal was dug around the city, giving the planning of this ancient city a spherical shape with a diameter of about 900 meters. The city center also has an old natural fountain [7]. Because Wiang Chet Lin city is located at the foot of the Doi Suthep mountain, the city has an area of high elevation on the west and tilted to the east. The western area is much higher than other areas. The ORLCM area is located at the boundary between the foothills of the Doi Suthep mountain and the Chiang Mai basin which is characterized by the great relief and steep slopes. The eastern of the Doi Suthep Ranges comprise of granite, granodiorite and diorite of Triassic age intruded Carboniferous and Silurian-Devonian sedimentary rocks [8,9]. Most of the area of the Chiang Mai basin contains the unconsolidated Quaternary alluvium. High terrace deposits containing thick sand and gravel beds of Lower Pleistocene-Pliocene age are located along the sides of the Chiang Mai Basin [10]. Fig. 1 shows the revised geological map from the Department of Mineral Resources of Thailand (DMR) [11] showing that most of the surveyed areas are in the granite area. There are three groundwater wells in the ORLCM area (Fig. 1): G1, G2 and G3. Drilling data from the three groundwater wells [12] shows the deposition of sediment layer (as clay, sand and gravel) from surface to the depth of about 60 meters overlaying the granite. The granite layer is at a depth from about 60 meters to the bottom of the groundwater wells at a depth of about 120 meters.

3. METHODOLOGY

3.1 Data acquisition

The 3D data set was obtained by combining 2D ERT data from 11 parallel survey lines (ProfileW1-W11). They were acquired in SE-NW direction with the line separation distance of 10 m and the line length of 200 m (Fig. 2a). The survey covers an area of 200×100 m^2. The 2D data were collected using a gradient electrode configuration (Fig. 2b). The electrode spacing "a" is 5 m, the separation factor of potential electrode (P1, P2) spacing "n" is from 1-4 and the separation factor of current electrode (C1, C2) spacing "s" is 10. Total number of datum points of each 2D ERT line is 512. Therefore, the total number of datum points in the 3D ERT data set in this area is 5,632.

Another 2D profile, called WL was acquired overlap on profile W2 with 400 m length and was carried out using the gradient array. The electrode spacing "a" of this line is 10 m, 20 m, and 30 m, a separation factor of potential electrode (P1, P2) spacing "n" is 1, 2 and 3 and separation factor of current electrode (C1, C2) spacing "s" is 10. This 2D line provides subsurface resistivity distribution at greater depth. Total number of datum points of this line is 504. Location and layout of inline 3D ERT survey and WL line are shown in Fig. 1 and 2.

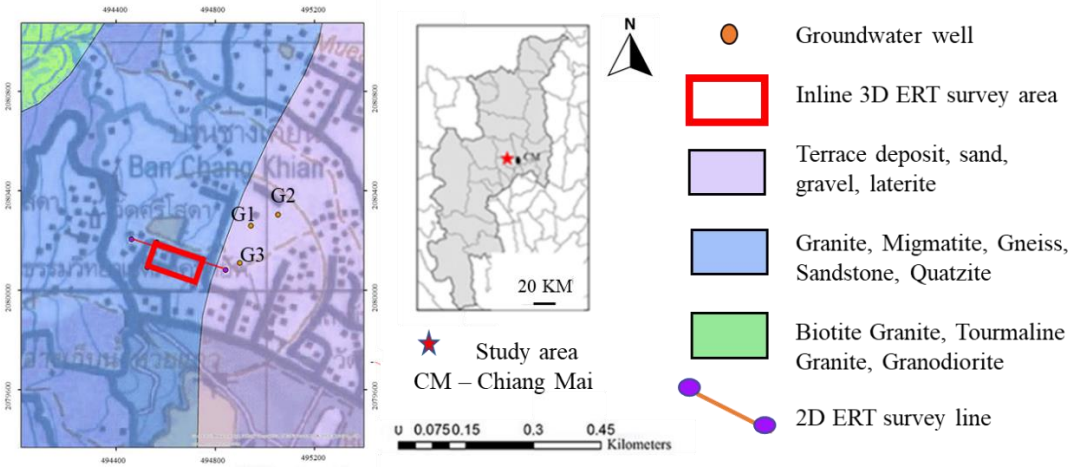

Fig. 1 Geologic map and location of the survey area in ORLCM 5, Chiang Mai [11].

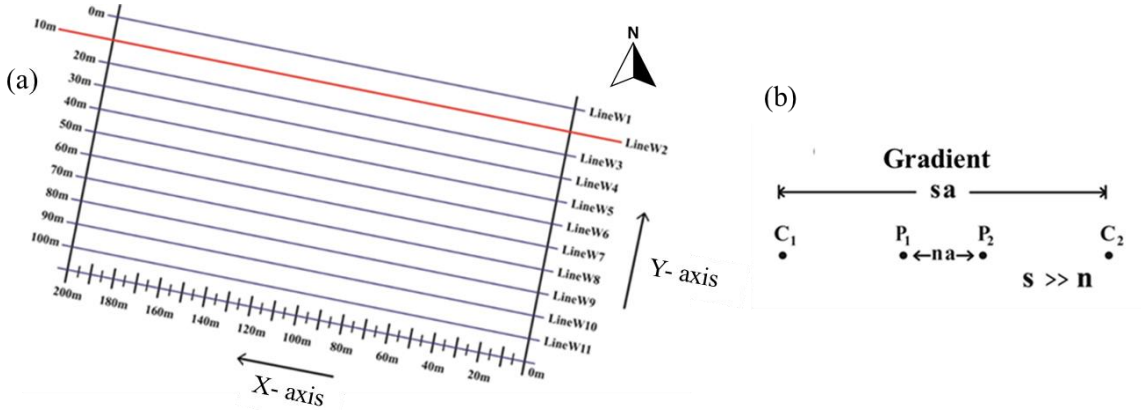

Fig. 2 (a) Layout of 11 parallel 2D ERT lines (LineW1-LineW11) used for combining into 3D ERT data set. Red line is Profile WL. (b) Gradient electrode array.

3.2 Data processing

Each raw data file was manually inspected for negative apparent electrical resistivity. Another data quality control was used to remove datum points with the standard deviation (SD) greater than 5 percent. Datum points with unreasonably high or low resistivity values are also manually eliminated by visual inspection. For all resistivity inversion models in this study, the smooth model inversion was used as an inversion method. The forward problem was solved using the finite element method with mixed type boundary condition. Forward equation solvers used in this study were the conjugate gradient (CG) solver for 3D forward modeling and the Cholesky decomposition (CD) for 2D forward modeling. L2-norm was used to stop any 2D and 3D inversion based on least squares methods such as damped least squares and smooth model inversion.

In this study the obtained 2D data were processed with EarthImager™ 2D. The combined 11 parallel 2D lines were inverted in EarthImager™ 3D.

3.3 Bedrock detection

For bedrock determination in this study, a similar edge detection technique to [5] and [6] were used. The steepest gradient (first derivative) and the Laplacian (second derivative) of the 3D ER data were calculated using Microsoft® Excel®. The method used to perform this calculation in Excel® is the finite difference method. The finite difference method was used to calculate the change in resistivity (ρ) between two data points to the change in x, y, and z directions in 3D ERT inverse model between each of those same datum points.

The first derivative can be interpreted as an instantaneous rate of change of the resistivity by,

$$\frac{\partial \rho}{\partial x} = \frac{(\rho_{n+1}-\rho_n)}{(x_{n+1}-x_n)} = \rho'_x \quad (1)$$

$$\frac{\partial \rho}{\partial y} = \frac{(\rho_{n+1}-\rho_n)}{(y_{n+1}-y_n)} = \rho'_y \quad (2)$$

$$\frac{\partial \rho}{\partial z} = \frac{(\rho_{n+1}-\rho_n)}{(z_{n+1}-z_n)} = \rho'_z \quad (3)$$

$$\nabla\rho(\mathrm{x},\mathrm{y},\mathrm{z}) = \frac{\partial \rho}{\partial x} + \frac{\partial \rho}{\partial y} + \frac{\partial \rho}{\partial z} \quad (4)$$

The second derivative can be interpreted as an instantaneous rate of change of the rate of change of the resistivity by,

$$\frac{\partial^2 \rho}{\partial^2 x} = \frac{\rho'_{x_{n+1}}-\rho'_{x_n}}{(x'_{n+1}-x'_n)} = \rho''_x \quad (5)$$

$$\frac{\partial^2 \rho}{\partial^2 y} = \frac{\rho'_{y_{n+1}}-\rho'_{y_n}}{(y'_{n+1}-y'_n)} = \rho''_y \quad (6)$$

$$\frac{\partial^2 \rho}{\partial^2 z} = \frac{\rho'_{z_{n+1}}-\rho'_{z_n}}{(z'_{n+1}-z'_n)} = \rho''_z \quad (7)$$

$$\nabla^2\rho(x,y,z) = \frac{\partial^2 \rho}{\partial x^2} + \frac{\partial^2 \rho}{\partial y^2} + \frac{\partial^2 \rho}{\partial z^2} \quad (8)$$

The steepest gradient method searches for maximum and minimum values in the first derivatives of ERT model. It considers a variation in gradient (first derivative) in the vertical (z) and horizontal (x, y) directions. Only the vertical direction is reasonable for estimation of a horizontal structure like a bedrock by using (3). This technique is less sensitive for vertical structures. It also has a disadvantage if multiple gradients are present such that it cannot discriminate between edges of structure. There are two steps to solve this problem; 1) if multiple gradients in the correct direction (i.e., decreasing resistivity with decreasing elevation) are present, then the steepest gradient is chosen because, in most cases, low-resistivity sediment layer are above the highly resistive bedrock and 2) if the gradients are of a similar magnitude, the deeper gradient will be picked as the lower lithological surface in the ERT inverse model. The deeper gradient is likely to be between the sediment fill and bedrock surface [6].

The Laplacian method searches for value of zero in the Laplacian (second derivate) of the resistivity images in the horizontal (x and y) and the vertical (z) directions and only vertical (z) direction. The Laplacian zero line can accurately define the sediment-bedrock edge.

3.4 Bedrock edge detection modeling

After calculating the bedrock edge from the 3D ERT inverse models by the steepest gradient and the Laplacian methods, the calculated data files can be displayed as an isosurface image of the bedrock edge detection model.

4. RESULTS

Geological interpretation of the inverted ERT data from the ORLCM area is based on the available geological data and ground water well information. It can be assumed that the bedrock at this study site is granite overlain by unconsolidated sediments. The ER values of unconsolidated sediments (clay, sand, and gravel) range from 1-1,050 Ohm.m and the ER values of granitic rock range from 100 – 106 Ohm.m. At this study site, the ER value lower than 450 Ohm.m was interpreted as unconsolidated sediments or sedimentary rock while the ER value higher than 450 Ohm.m was interpreted as the bedrock (granite).

4.1 2D ERT results and interpretation

The inverted 2D ERT profiles from the ORLCM area include 11 profiles called W1 to W11 and WL. Note that profile W1 to W11 are 200 m in length while profile WL is 400 m in length where 200 m distance in the center of this profile overlaps profile W2. Depth of investigation from profiles W1 to W11 is 38.2 m, and from profile WL is 57 m. A high resistivity area of greater than 450 Ohm.m is presented in all the 2D ERT profiles from north to south. This continuous zone of such high resistivity was interpreted as the granite bedrock. Notice a dome-like structure of the high resistivity zone appeared at the center of the 2D ER profiles W1 to profile W7 but cannot be seen on profiles W8 to W11. Other areas where the resistivity values lower than 450 Ohm.m were interpreted as unconsolidated sediment. The low resistivity zones are on the top of the bedrock. Depth to the bedrock varies from 7.5 m to 45 m. Deeper bedrock appears on the southeastern side of the site, while shallower bedrock can be seen in the middle of the site. The 2D ERT profiles W8, W9 and W10 have very high ER values at surface distance range 100 to 130 m and at depth of 0 to 10 m. This may be due to a high resistive surface area of the old concrete floor found at the site. Profile WL is overlapped at the distance of 100 m to 300 m with the profile W2 at the distance of 0 to 200 m in the same direction. This profile shows depth of up to 64 m. This profile shows that the bedrock found on profile W2 continues at a shallower level. All 2D ERT results were shown that the granite surface declines about 10.48 degree from the west (the foothills of Suthep Mountain) to the east (Chiang Mai basin). Sediment layer overlaying the granite at the study area is due to an alluvial fan deposit of the sediments from Doi Suthep Mountain. Some 2D ERT profiles from this study are displayed in Fig. 4. Fig. 5 presents images of inverted 3D ERT data obtained from combining 11 lines of 2D ERT data at the ORLCM study area. This 3D ERT data cover an area of 200x100 m^2 and provide an investigation depth of 42 m. The ER value range obtained from inversion is 12 to 7,531 Ohm.m. The X direction side shows higher ER value than 450 Ohm.m (yellow to red color scale). This may indicate the granite. Other areas where the resistivity values lower than 450 Ohm.m (blue and green color scale) were interpreted as unconsolidated sediments. Internal ER structure of the bedrock can be seen in Figs. 5a and 5b. Vertical slices of the 3D ERT data are presented in Fig. 5b in the Y direction, respectively, where internal ER structure can be seen the bedrock.

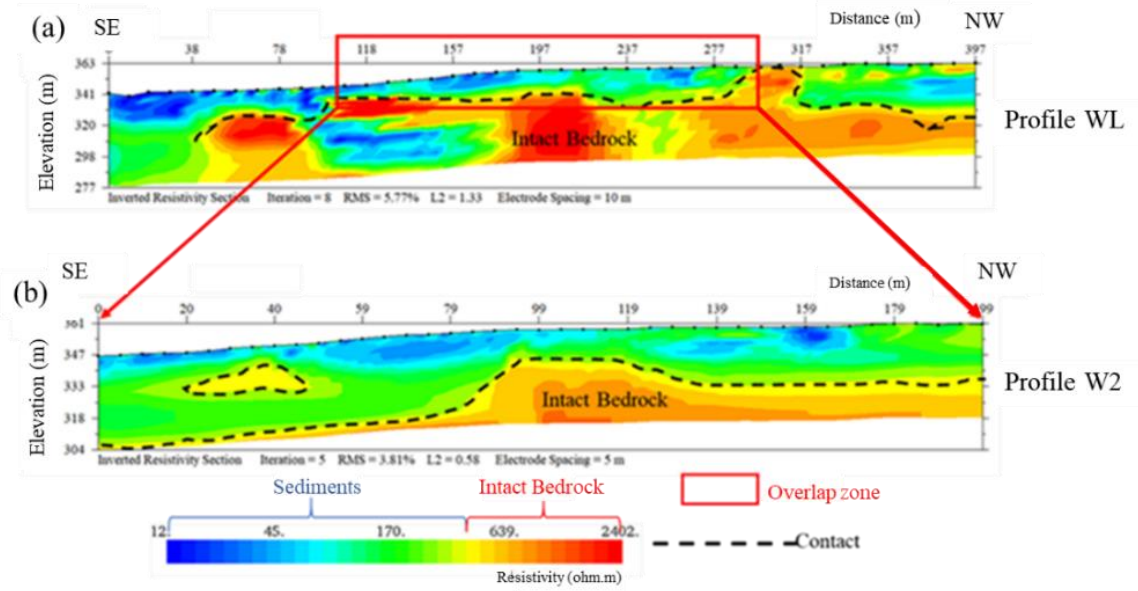

Fig. 4 Inverted 2D ERT profiles of the ORLCM study area. (a) Profile WL and (b) Profile W2.

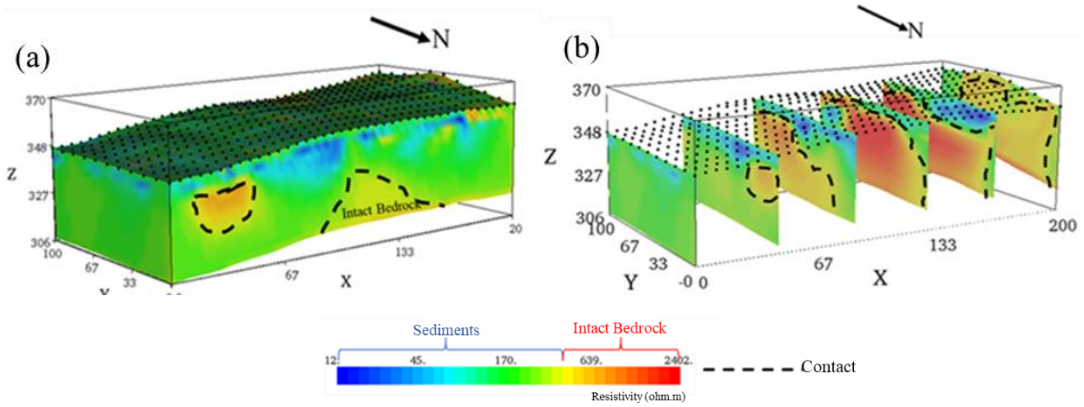

Fig. 5 3D ERT inverse images at ORLCM study area. (a) 3D ERT inverse images. (b) vertical slices in Y-direction.

4.2 Depth to bedrock determination

In the inverted ERT data at the ORLCM study site, an area where the ER value higher than 450 Ohm.m is interpreted as the granitic bedrock. Fig. 6 shows the isoresistivity value of 450 Ohm.m in the inverted 3D ER data. The depth range of this isoresistivity is 13 to 28 m with surface distance range of 5 to 200 m. Other shallower areas of 450-Ohm.m isosurface, due to other high resistive zones at near surface, was caused by the remains of buildings in the survey area. The depth of the granite in the isoresistivity surface is different from the depth of the granite found in the groundwater wells in the area. This is because the groundwater wells are located in an area of the Chiang Mai Basin where sediment is thickly deposited, but the ER survey area is at the foothill of Doi Suthep where there is less deposition of sediments. Therefore, the data from the ground wells were used only to identify the type of Earth material in the study area.

First derivative in X, Y, and Z directions of the inverted 3D ERT data from ORLCM area gives the steepest gradient of 64.94 Ohm which is suitable to be at the edge of the bedrock. An image of the first derivative isosurface value of 64.94 Ohm, is shown in Fig. 7a. Depth of the main area of the first derivative isosurface ranges from 20 to 30 m. Other shallower areas of this isosurface value of 64.94 Ohm may due to other high resistive zones at near surface which was caused by the remains of buildings in the survey area.

First derivative in Z direction of the inverted 3D ERT data from ORLCM area gives the steepest gradient value of -45.085 Ohm which is best suitable to be the edge of the bedrock. An image of the first derivative isosurface value of -45.085 Ohm is shown in Fig. 7b. Depth of the main area of the first derivative isosurface ranges from 20 to 30 m. Other shallower areas of this isosurface value of -45.085 Ohm may be due to other high resistive zones at near surface, which was caused by the remains of buildings in the survey area.

Second derivative in X, Y, and Z directions of the inverted 3D ERT data from ORLCM area gives an isosurface value of 0 $Ohm.m^{-1}$ as shown in Fig. 7c. Depth of the main area of the second derivative isosurface ranges from 20 to 40 m but the isosurface value characteristic of 0 $Ohm.m^{-1}$ differs from the isoresistivity value surface of 450 Ohm.m in Fig. 6. Because the of complexity of subsurface geological variations in the ORLCM area, second derivative produces many false interfaces (isosurface value of 0)

Second derivative in Z direction of the inverted 3D ERT data from ORLCM area gives an isosurface value of 0 $Ohm.m^{-1}$ as shown in Fig. 7d. Depth of the main area of the second derivative isosurface ranges from 20 to 40 m but the isosurface value characteristic of 0 $Ohm.m^{-1}$ differs from the isoresistivity surface of 450 Ohm.m in Fig. 6. Because of the complexity of subsurface geological variations in the ORLCM area, second derivative produces many false interfaces.

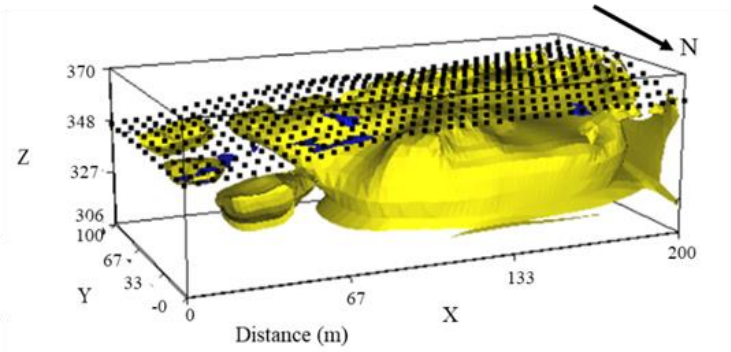

Fig. 6 The 450 Ohm.m isoresistivity surface of the inverted 3D ER data of the ORLCM study area.

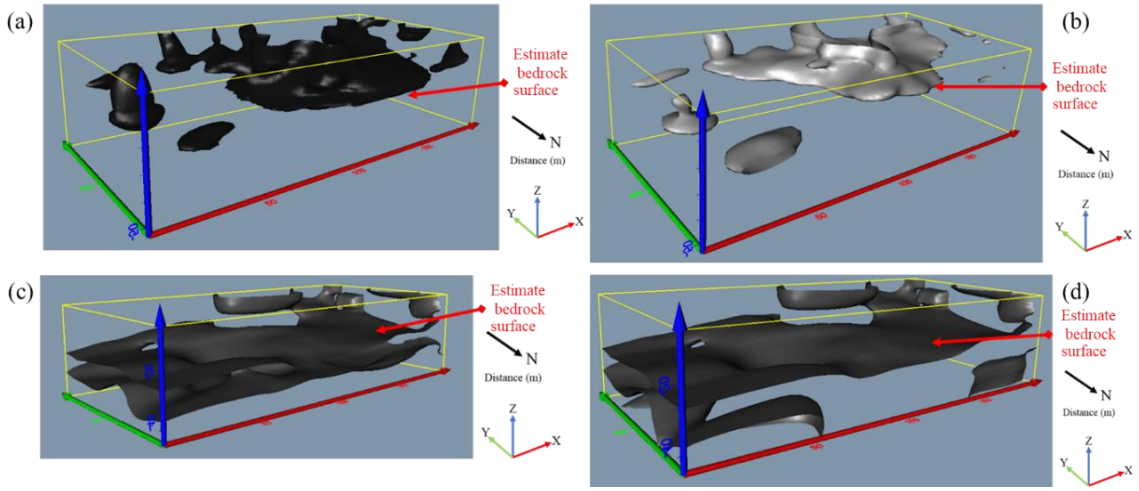

Fig. 7 Images created by applying edge detection techniques to the inverted 3D ERT data from ORLCM area. (a) Isosurface image of first derivative in X, Y, and Z directions. (b) Isosurface image of first derivative in Z direction. (c) Isosurface image of second derivative in X, Y and Z directions (d) Isosurface image of second derivative in Z direction.

5. DISCUSSION

The first derivative can be interpreted as a rate of change and the second derivative can be interpreted as a rate of change of the rate of change [13]. The steepest gradient value of the first derivative in ERT data is the highest value of the rate of change correlated with the strongest contrast between ER of bedrock and topsoil. The inflection point of second derivative is 0. This point is a point of a curve at which the change in the direction of curvature occurs [14]. A change between high to low value or a change between low to high value corresponds with edge of transition zone in ERT model. The depths of bedrock from applying the first derivative methods in x, y, and z directions and only in z direction to the 3D ERT data from ORLCM study area, are more accurate than the depth of bedrock from applying the second derivative method. This area has complex geology. Many false zero interfaces were produced by the Laplacian method because the second derivative of ERT data produces many false interfaces (zero). False zero interfaces are not related to the contact between the bedrock and sediment.

Based on the results of applying edge detection techniques to the 3D ERT data from this site, two factors influencing depth accuracy are identified: 1) The accuracy of the 3D ERT data. Inaccurate 3D ERT data results in inaccurate estimates of the depth to the bedrock. 2) The resolution and sensitivity of the model. These qualities decrease with depth and in boundary regions, which, in turn, affect the depth estimation of the bedrock using edge detection techniques. Therefore, it is crucial to plan the survey properly, considering factors such as the selection of the 3D data survey type (full 3D ERT or inline 3D ERT survey), electrode configuration, electrode spacing, line spacing, and other relevant parameters.

The accuracy of 3D ERT inversion has a direct impact on the effectiveness of edge detection techniques. Therefore, it is imperative to further validate the accuracy of 3D ERT inversion. To accomplish this, an investigation should be conducted using synthetic data that models sediment layers deposited on granite bedrock, including surface topography. Once the accuracy of 3D ERT inversion is confirmed, the application of edge detection techniques to this dataset can proceed in the subsequent step.

6. CONCLUSIONS

Edge detection techniques by the steepest gradient and the Laplacian methods applied in this study give different depths to bedrock results for the same inverted 3D ERT data set. Depth to bedrock for this study area from the steepest gradient method in only vertical (Z direction) corresponds to those interpreted from the inverted 2D and 3D ERT data. As a result, from this study, the edge detection techniques can determine the edge between the topsoil and bedrock, and can accurately visualize the orientation and shape of the bedrock in the 3D ERT data. The utilities of this study can be applied in accretion with foundation design in the construction industry. Edge detection techniques can also be applied in 3D ERT data for other purposes such as determining the extent of contamination in a waste pit or characterizing a sinkhole.

ACKNOWLEDGEMENTS

We are grateful to the Office of Regional Livestock 5, Chiang Mai, for allowing us to use their property as the study area.

REFERENCES

[1] Currier L.W., The seismic method in subsurface exploration of highway and foundation sites in Massachusetts; Available at: https://pubs.er.usgs.gov/publication/cir426.

[2] Pánek T., Hradecký J., Smolková V., Šilhán K., Minár J. and Zernitskaya V., *Geomorphology*, 2010; **120**: 233–247. DOI 10.1016/j.geomorph.2010.03.033.

[3] Rucker D.F., Fink J.B. and Loke M.H., *Journal of Applied Geophysics*, 2011; **74**: 242-254. DOI 10.1016/j.jappgeo.2011.06.005.

[4] Sherrod L., Simpson E.L., Higgins R., Miller K., Morgano K., Snyder E., and Vales D., *Sedimentary Geology*, 2016; **344**: 160–174. DOI 10.1016/j.sedgeo.2016.02.005.

[5] Hsu H.L., Yanites B.J., Chen C.C. and Chen Y.G., *Geomorphology*, 2010; **114**: 406–414. DOI 10.1016/j.geomorph.2009.08.004.

[6] Chambers J.E., Wilkinson P.B., Wardrop D., Hameed A., Hill I., Jeffrey C., Loke M.H., Meldrum P.I., et al., *Geomorphology*, 2012; **177–178**: 17–25. DOI 10.1016/j.geomorph.2012.03.034.

[7] Guntang I., *NAJUA: Design and Built Environment*, 2015; **29**: 87-104; Available at: https://so04.tci-thaijo.org/index.php/NAJUA-Arch/article/view/44221.

[8] Beckinsale R.D., Suensilpong S., Nakapadungrat S., and Walsh J.N., *Journal of the Geological Society*, 1979; **136**: 529-540. DOI/10.1144/gsjgs.136.5.0529.

[9] Hutchison C.S. Multiple Mesozoic Sn-W-Sb granitoids of southeast Asia; in Roddick J.A., *Circum-Pacific Plutonic Terranes*, Geological Society of America Memoir 1983: 35-60.

[10] Wattananikorn K., Beshirt J.A. and Nochaiwong A., *Journal of Southeast Asian Earth Sciences*, 1995; **12**: 53-64. DOI 10.1016/0743-9547(95)00022-4.

[11] Department of Mineral Resources Thailand, North Geological maps by province; Available at http://www.dmr.go.th/download/pdf/North/Chiangmai.pdf.

[12] Department of Groundwater Resource Thailand, PASUTARA Thailand's groundwater data base; Available at http://dgr.go.th/newpasutara/xml/tmapdetail.php?wellID=CM286-288.

[13] Department of Mathematics, Damouth Collage, The First and Second Derivatives; Available at https://math.dartmouth.edu/opencalc2/cole/lecture8.pdf.

[14] Reinholz D., The Second Derivative; Available at https://www.ocf.berkeley.edu/~reinholz/ed/07fa_m155/lectures/second_derivative.pdf.